Dalton Transactions

PAPER

View Article Online
View Journal | View Issue

Cite this: *Dalton Trans.*, 2014, **43**, 4295

Tuning ligand electronics and peripheral substitution on cobalt salen complexes: structure and polymerisation activity†‡

Linus Chiang,[a] Laura E. N. Allan,[b] Juan Alcantara,[a] Michael C. P. Wang,[a] Tim Storr*[a] and Michael P. Shaver*[b]

Received 9th July 2013,
Accepted 9th September 2013

DOI: 10.1039/c3dt51846a

www.rsc.org/dalton

A series of cobalt salen complexes, where salen represents an N_2O_2 bis-Schiff-base bis-phenolate framework, are prepared, characterised and investigated for reversible-termination organometallic mediated radical polymerisation (RT-OMRP). The salen ligands contain a cyclohexane diimine bridge and systematically altered *para*-substituted phenoxide moieties as a method to examine the electronic impact of the ligand on complex structure and reactivity. The complexes are characterised by single crystal X-ray diffraction, cyclic voltammetry, X-ray photoelectron spectroscopy, electron paramagnetic resonance spectroscopy and computational methods. Structural studies all support a tailorable metal centre reactivity altered by the electron-donating ability of the salen ligand. RT-OMRP of styrene, methyl methacrylate and vinyl acetate is reported and suggests that cobalt–carbon bond strength varies with the ligand substitution. Competing β-hydrogen abstraction affords long-chain olefin-terminated polymer chains and well controlled vinyl acetate polymerisations, contrasting with the lower temperature associative exchange mechanism of degenerative transfer OMRP.

Introduction

Metal complexes of tetradentate salen (salen is a common abbreviation for N_2O_2 bis-Schiff-base bis-phenolates) ligands have received considerable attention in transition metal chemistry due to their relative ease of synthesis, ability to form stable complexes with many metals in a variety of oxidation states and versatility as catalysts for important organic transformations.[1–9] Notable examples of catalysis include Mn salen olefin epoxidation,[1,2] Co salen hydrolytic kinetic resolution of epoxides,[10] Co salen enantioselective polymerisation of epoxides,[11,12] and Cr/Co salen coupling of CO_2 and epoxides.[5,9,13] The modular synthesis of the salen framework allows easy tuning of both sterics and electronics, providing a means to study how subtle changes to the ligand framework influence reactivity.

In many cases the steric and electronic properties of the salen ligand exerts a profound effect on the reaction outcome. For example, enantiomeric excess (ee) values for the Mn salen – catalysed asymmetric epoxidation of pro-chiral olefins depends on the nature of the chiral diimine bridge and the identity of the *ortho*- and *para*-ring substituents.[2,14–16] While the *ortho*-ring substituents primarily provide steric bulk to influence substrate approach, the electron-donating ability of the *para*-ring substituents has a significant effect on the reaction outcome by altering the position of the transition state along the reaction coordinate.[14,15] In the case of Mn salen complexes, electron-donating *para*-ring substituents lead to a late transition state and afford the highest ee values. A smaller effect of the *para*-ring substituents (Br, H, *t*Bu) is observed for Co salen copolymerisation of propylene oxide and CO_2, with the *t*Bu derivative showing the highest regioselectivity.[17] Similar to the Mn salen results, electron-donating substituents increased the rate of copolymer formation for Cr salen catalysed cyclohexene oxide/CO_2 copolymerisation.[5,18] These results highlight the influence of the electron-donating ability of the *para*-ring substituents on the catalytic activity of the metal centre.

We were interested in studying the polymerisation activity of a series of Co salen complexes wherein we have varied the electron-donating ability of the *para*-ring substituents (NMe_2 > OMe > *t*Bu > NO_2) (Chart 1). In particular, the role these

[a]*Department of Chemistry, Simon Fraser University, 8888 University Drive, Burnaby, BC V5A 1S6, Canada. E-mail: tim_storr@sfu.ca*
[b]*School of Chemistry, University of Edinburgh, Joseph Black Building, West Mains Road, Edinburgh, EH9 3JJ, UK. E-mail: michael.shaver@ed.ac.uk; Tel: +44 (0) 131 650 4726*

† Celebrating 300 years of Chemistry at Edinburgh.

‡ Electronic supplementary information (ESI) available: Full XPS spectra for CoSal[R1,R2], DFT metrical parameters, further polymerisation data and summary of crystallographic data. CCDC 948259. For ESI and crystallographic data in CIF or other electronic format see DOI: 10.1039/c3dt51846a

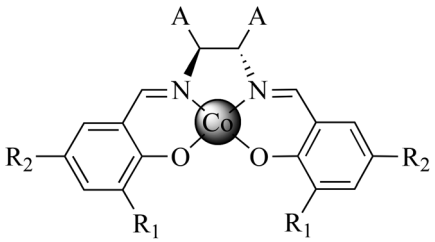

A = $(CH_2)_4$

CoSal$^{tBu, NO2}$: R_1 = tBu, R_2 = NO_2

CoSal$^{tBu, tBu}$: R_1 = tBu, R_2 = tBu

CoSal$^{tBu, OMe}$: R_1 = tBu, R_2 = OMe

CoSal$^{tBu, NMe2}$: R_1 = tBu, R_2 = NMe_2

CoSal$^{H, tBu}$: R_1 = H, R_2 = tBu

Chart 1 Structures of the Co Schiff-base complexes CoSal^{R1,R2}.

complexes could play in controlling organometallic mediated radical polymerisation (OMRP) is important.[19] In this variant of controlled radical polymerisation, the fast and reversible homolytic cleavage of a metal–carbon bond is exploited to lower radical concentrations and control the properties of the polymer products. OMRP may proceed through reversible termination (RT), where a transition metal complex acts as a reversible spin-trap to deactivate the propagating chains, or through degenerative transfer (DT) whereby associative exchange between an active radical and a metal-bound radical of the dormant species takes place. Cobalt complexes dominate the OMRP literature,[20] imparting the best control, although the development of other metals as OMRP mediators is a recent topic of interest.[19,21–25]

Early cobalt OMRP systems were based on nitrogen donors, such as porphyrins,[26–29] which were particularly efficient for the OMRP of acrylates. A more recent report examined a series of 1,3-bis(2-pyridylimino)isoindolate ligands, structurally related to porphyrins, but lacking a fourth N-donor.[30] These complexes were active for acrylate polymerisation but did not show the anticipated structure–activity relationship, leading the authors to conclude that the cobalt–carbon bond was decoupled from the ligand substituents and so inclusion of electron-withdrawing or electron-donating groups had no effect on the polymerisation behaviour. Cobalt species incorporating oxygen donors, such as bis-acetylacetonate Co(II) and related complexes,[19–22] are very efficient for the OMRP of vinyl acetate[31–36] and careful choice of reaction conditions has allowed expansion of the monomer scope to include acrylates,[37–39] acrylonitrile,[40–43] other vinyl ester monomers[44,45] and *N*-vinylpyrrolidone.[44,46] The use of mixed N,O-donor systems in cobalt-mediated OMRP is limited to reports on the β-ketoiminates,[47,48] which exert reasonable control over methyl acrylate and vinyl acetate polymerisation, and a very recent report on the highly efficient degenerative transfer OMRP of vinyl acetate and methyl acrylate mediated by cobalt(II) [*N*,*N*-bis(3,5-di-*tert*-butylsalicylidene)-1,2-cyclohexanediamine],[49] (CoSal^{tBu,tBu}), which was published during the course of our study.

To complement these recent efforts by Liao *et al.* we have focused our efforts on the more challenging reversible-termination (RT) OMRP methodology. In this work we have investigated the electronic structure of a series of Co(II) salen complexes where we have varied the *para*-ring substituents (Chart 1). We have shown that the *para*-ring substituents influence both the electron density at the metal centre as well as the overall reactivity *via* increasing stability of the Co(II) forms in the order of NMe_2 > OMe > *t*Bu > NO_2. The more electron-donating substituents should thus increase the concentration of propagating radicals in the system and the use of the Co(II) salen complexes in RT-OMRP is reported.

Results and discussion

Synthesis and characterisation

The Co complexes CoSal^{R1,R2} were synthesised in good yields from the metallation of the corresponding ligands H_2Sal^{R1,R2} with $Co(OAc)_2{\cdot}4H_2O$.[50–55] CoSal^{tBu,NO2} yielded crystals suitable for X-ray analysis, using THF–pentane as the recrystallisation solvents. The molecular structure of CoSal^{tBu,NO2}·THF is shown in Fig. 1 and selected crystallographic data for the complex are presented in Table 1. CoSal^{tBu,NO2} exhibits an essentially square planar geometry at the Co centre with a molecule of THF weakly coordinated in the axial position ($Co–O_{THF}$ ~ 2.21 Å). The dihedral angle between the N–Co–O planes is 9°, likely due to the steric interaction between the two *ortho* *t*-butyl groups.

Electrochemistry

Redox processes for CoSal^{tBu,R2} were probed by cyclic voltammetry (CV) in CH_2Cl_2 using tetra-*n*-butylammonium perchlorate ($^nBu_4NClO_4$) as the supporting electrolyte. CoSal^{tBu,NO2} was not soluble in CH_2Cl_2 and thus the CV experiments were completed in THF. Three quasi-reversible, one-electron redox

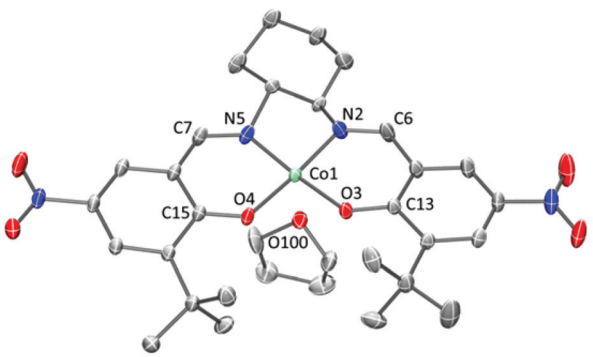

Fig. 1 POV-ray representation (50% probability) of CoSal^{tBu,NO2}·THF, excluding hydrogen atoms. Selected interatomic distances (Å) and angles (°): Co(1)–O(4), 1.901; Co(1)–O(3), 1.895; Co(1)–N(5), 1.876; Co(1)–N(2), 1.874; N(5)–C(7), 1.292; N(2)–C(6), 1.288; O(4)–C(15), 1.296; O(3)–C(13), 1.291; Co(1)–O(100), 2.211; O(3)–Co(1)–O(4), 86.9(4); O(4)–Co(1)–N(5), 93.5(7); O(3)–Co(1)–N(2), 93.4(8); N(2)–Co(1)–N(5), 85.2(7).

Table 1 Experimental and calculated[a] metrical parameters for CoSal^{tBu,NO2}·THF in Å

Bond/distance	CoSal^{tBu,NO2}·THF (Å) experimental	CoSal^{tBu,NO2}·THF (Å) calculated
Co(1)–O(4)	1.901	1.901
Co(1)–O(3)	1.895	1.900
Co(1)–N(5)	1.876	1.884
Co(1)–N(2)	1.874	1.893
Co(1)–O(100)	2.211	2.282
N(5)–C(7)	1.292	1.296
N(2)–C(6)	1.288	1.297
O(4)–C(15)	1.296	1.295
O(3)–C(13)	1.291	1.293

[a] See Experimental section for calculation details.

processes were observed for R_2 = *t*Bu, OMe and NMe_2, where only a single redox process was observed for $R_2 = NO_2$ (Fig. 2). The reversibility of these processes was evaluated *via* comparison of the peak-to-peak difference ($|E_{pa} - E_{pc}|$) for a specific redox process to that of the Fc^+/Fc couple under identical conditions (Table 2). The redox potentials *versus* ferrocenium/ferrocene (Fc^+/Fc) are reported in Table 2. The three redox couples can be assigned to the metal centre Co(II)/Co(III) and the two redox-active phenolate moieties. The redox chemistry of the *t*Bu, and OMe derivatives have been reported previously with the first redox process assigned as a one-electron Co(II)/Co(III) couple (Fig. S1‡).[53,56] The more positive redox potential for the NO_2 derivative is due to the presence of electron-withdrawing groups in the *para* position. The positive shift in the potential for the NO_2 derivative (and the use of THF as the solvent) results in only one of the redox processes being visible by CV in this work. Overall there is a clear shift in the redox potentials towards more negative values as the electron-donating ability of the *para*-substituents is increased (NMe_2 > OMe > *t*Bu > NO_2). Modulation of the electron-donating ability of the salen ligands is subsequently shown to have an effect on the polymerisation activity of the Co complexes (*vide infra*).

X-ray photoelectron spectroscopy

The electronic structures of the Co complexes CoSal^{tBu,R2} were investigated by XPS (Fig. 3). Referenced to the C 1s binding energy, the Co $2p_{3/2}$ and Co $2p_{1/2}$ binding energies (Table 3) for all four CoSal^{tBu,R2} complexes indicate a common 2+ oxidation state for Co.[57–59] Comparing the binding energies a general trend is observed: as the electron-donating ability of the *para*-ring substituents is increased, there is a decrease in the Co $2p_{3/2}$ and $2p_{1/2}$ binding energies. These data are further evidence for the influence of the *para*-ring substituents on the electronics at the metal centre.

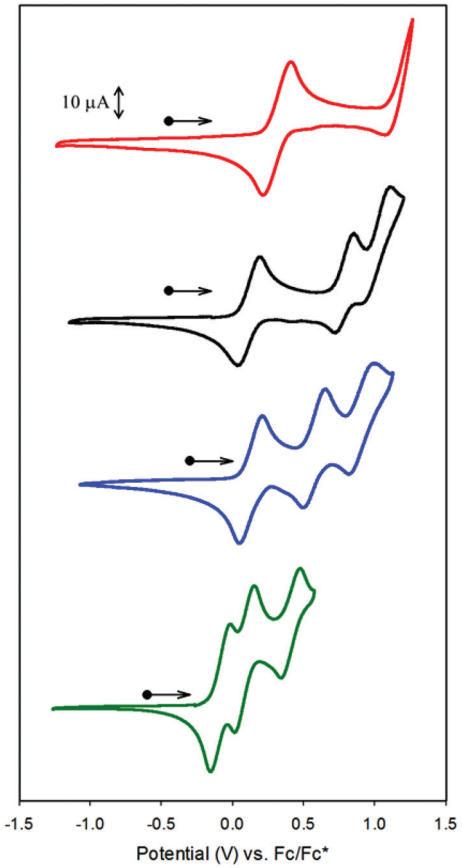

Fig. 2 Cyclic voltammograms of CoSal^{tBu,R2} (red: $R_2 = NO_2$; black: R_2 = *t*Bu; blue: R_2 = OMe; green: $R_2 = NMe_2$) *versus* Fc^+/Fc.

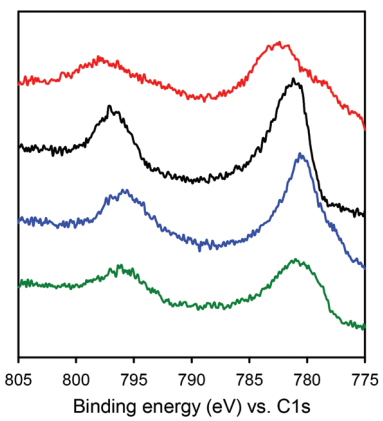

Fig. 3 X-ray photoelectron spectroscopy (XPS) spectra of CoSal^{tBu,R2} compounds showing the Co $2p_{3/2}$ and $2p_{1/2}$ binding energies (red: $R_2 = NO_2$; black: R_2 = *t*Bu; blue: R_2 = OMe; green: $R_2 = NMe_2$). Full spectra shown in Fig. S2.‡

Table 2 Redox potentials for CoSal^{tBu,R2} *versus* Fc^+/Fc[a] (1 mM complex, 0.1 M $^nBu_4NClO_4$, scan rate 100 mV s^{-1}, CH_2Cl_2, 233 K)

CoSal^{tBu,R2}	$E^1_{1/2}$ (mV)	$E^2_{1/2}$ (mV)	$E^3_{1/2}$ (mV)
$R_2 = NO_2$ [b]	310 (190)	—	—
R_2 = *t*Bu	110 (160)	780 (130)	1020 (190)
R_2 = OMe	130 (160)	570 (160)	910 (180)
$R_2 = NMe_2$	−90 (140)	80 (140)	400 (130)

[a] Peak-to-peak differences in brackets ($|E_{pa} - E_{pc}|$ in mV). Peak-to-peak difference for the Fc^+/Fc couple at 233 K is 80 mV. [b] Solvent = THF.

Table 3 Co (2p) binding energies *vs.* C(1s) (284.2 eV)

CoSal^{tBu,R2}	Binding energy (eV)	
	Co ($2p_{3/2}$)	Co ($2p_{1/2}$)
R_2 = NO_2	797.6	782.8
R_2 = *t*Bu	796.8	781.1
R_2 = OMe	795.7	780.4
R_2 = NMe_2	795.6	780.6

Electron paramagnetic resonance

The X-band EPR spectra of the complexes CoSal^{tBu,R2} were studied at 20 K and are consistent with a low spin Co(II) (S = 1/2) ground state (Fig. 4).[60,61] Based on previous work of Daul *et al.*, and the fitting of the experimental EPR data, the CoSal^{tBu,tBu}, CoSal^{tBu,OMe} and CoSal^{tBu,NMe2} derivatives exhibit a $|yz, {}^2A_2\rangle$ ground state in frozen PhMe (Table 4). This result is consistent with other reported 4-coordinate Co(II) salen complexes.[60,61] The CoSal^{tBu,NO2} derivative was not soluble in PhMe, and thus the isolated THF adduct was dissolved in a 2 : 1 mixture of PhMe–CH_2Cl_2 and subsequently frozen for EPR analysis. The observed spectrum displays a different pattern in comparison to the *t*Bu, OMe, and NMe_2 analogues (Fig. 4), suggesting a different ground state for this complex. EPR fitting analysis provides evidence for a $|z^2, {}^2A_1\rangle$ ground state for CoSal^{tBu,NO2} under these conditions, consistent with a 5-coordinate structure (likely THF adduct). This analysis is further corroborated by theoretical calculations (*vide infra*).

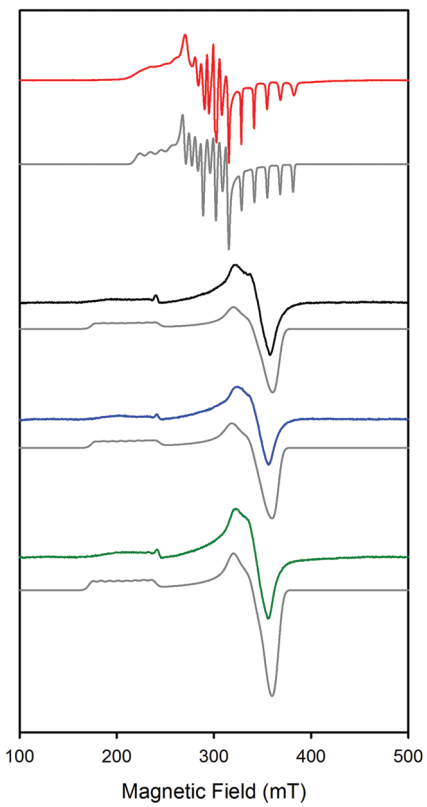

Fig. 4 X-band EPR spectra of CoSal^{tBu,R2}. Red: R_2 = NO_2, ν = 9.384 GHz; black: R_2 = *t*Bu, ν = 9.383 GHz; blue: R_2 = OMe, ν = 9.383 GHz; green: R_2 = NMe_2, ν = 9.385 GHz. Grey spectra are respective simulations. Conditions: power = 2.0 mW; modulation frequency = 100 kHz; modulation amplitude = 0.4 mT; T = 20 K.

Table 4 EPR parameters for the CoSal^{tBu,R2} complexes (R_2 = NO_2, *t*Bu, OMe and NMe_2)

	g_x	g_y	g_z	A_x (Co)[a]	A_y (Co)[a]	A_z (Co)[a]
CoSal^{tBu,tBu} [b,c]	3.21	1.88	1.98	400	80	125
CoSal^{tBu,OMe} [c]	3.21	1.89	1.99	400	80	125
CoSal^{tBu,NMe2} [c]	3.19	1.89	1.99	400	80	125
CoSal$^{tBu\ NO2}$ [d]	2.56	2.30	2.00	410	196	346

[a] Estimated values due to large g and A strain (A in MHz). [b] See ref. 59. [c] The fits for *t*Bu, OMe and NMe_2 are identical within experimental error. [d] Solvent 2 : 1 CH_2Cl_2–PhMe.

Theoretical analysis

Density functional theory (DFT) calculations of the CoSal^{tBu,R2} complexes provided further insight into the geometric and electronic structure of these complexes. We first compared the optimised geometry for the CoSal^{tBu,NO2}·THF complex with the experimental X-ray metrical data (Table 1). The calculations reproduce the coordination sphere bond lengths to within ±0.02 Å. In the absence of the THF molecule, the predicted coordination sphere bond lengths differ significantly from the experimental data. The calculations of the neutral square planar Co(II) complexes provided further details of the effect of the peripheral substituents on the metal centre. Mulliken population analysis[62,63] predicts the lowest partial charge at Co (0.78) for CoSal^{tBu,NMe2} and the highest partial charge at Co (0.80) for CoSal^{tBu,NO2} consistent with the expected electronic effects of the *para*-ring substituents.

We further investigated the electronic structure of the CoSal^{tBu,R2} complexes and in particular the nature of the singularly occupied molecular orbital (SOMO). Based on the EPR data and fitting, the NMe_2, OMe, and *t*Bu derivatives display a common $|yz, {}^2A_2\rangle$ ground state.[60,61] The DFT calculations predict correctly a d_{yz}-containing SOMO for these three derivatives (Fig. 5). In addition, without the axial THF molecule the NO_2 derivative also displays a d_{yz} SOMO (Fig. S3‡). In contrast, the 5-coordinate THF adduct CoSal^{tBu,NO2}·THF exhibits a $|z^2, {}^2A_1\rangle$ ground state based on the EPR analysis. The DFT calculation for the THF adduct predicts correctly a d_{z^2} SOMO for this analogue (Fig. 5). Axial ligand binding in this case raises the energy of the d_{z^2} orbital in comparison to d_{yz}, resulting in the change in electronic ground state.

The 5-coordinate X–Co(III)Sal complexes (X = 1-phenylethane) were investigated *via* computations to better understand the influence of the *para*-ring substituents on the axial Co–C bond strength. The Co–C bond dissociation energies (BDE) were calculated by subtracting the energy of the X–Co(III)-

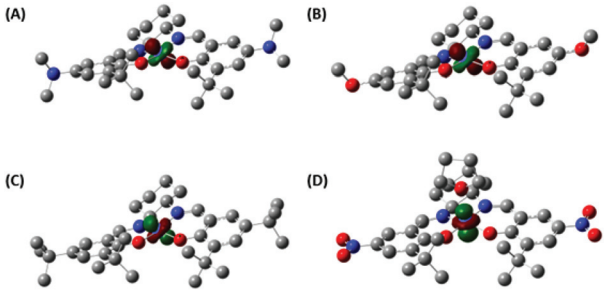

Fig. 5 Predicted singularly occupied molecular orbital (d_{yz}) for the Co(II) salen complexes, except the THF adduct of CoSal^{tBu,NO2} (d_{z^2}): (A) CoSal^{tBu,NMe2}; (B) CoSal^{tBu,OMe}; (C) CoSal^{tBu,tBu}; (D) CoSal^{tBu,NO2}·THF. See the Experimental section for calculation details.

Sal reactant from the sum of the energies of the products as shown in eqn (1).

$$X\text{–}Co(III)Sal^{tBu,R} \rightarrow Co(II)Sal^{tBu,R} + X^{\bullet} \quad (1)$$

For this series of calculations the BP86 functional was used,[64] based on prior work by Kozlowski *et al.* on alkyl-Co(III) macrocycles.[65–67] The Co–C BDE for the NO_2 derivative (15.4 kcal mol^{-1}) was predicted to be at least 1.3 kcal mol^{-1} higher than the values for the *t*Bu (14.1 kcal mol^{-1}), OMe (13.7 kcal mol^{-1}) and NMe_2 (13.3 kcal mol^{-1}) derivatives. The calculations predict the highest Co–C BDE for the NO_2 derivative, consistent with the electron-withdrawing *para*-substituents and resultant increased Lewis acidity at the metal centre. The predicted BDE values are lower than those previously reported for alkyl cobalt salen complexes (methyl, ethyl, *etc.*), likely due to the increased steric bulk of 1-phenylethane and presence of an additional axial ligand in the previous work.[68] Overall, the calculated Co–C BDE decrease as the electron-donating ability of the *para*-substituents is increased in the series.

Organometallic mediated radical polymerisation

Although recent research has significantly expanded the number of active systems in OMRP,[19,21,22] ligand design has an important role to play in increasing both the monomer scope and efficacy of OMRP catalysts. While the effect of carbon–halogen bond strengths on atom transfer radical polymerisation (ATRP) has been studied both experimentally and computationally, no similar data have been compiled for OMRP systems. Few investigations of systematic variation of ligand substituents have been reported, but a better understanding of the role of the metal–carbon bond strengths will facilitate improved control and tunability of polymerisations. To clarify the impact of bond strength, we wished to investigate our series of CoSal^{tBu,R2} complexes for reversible termination OMRP, with the strong electronic variation anticipated to significantly alter the cobalt–carbon bond strengths, potentially allowing us to tune our system for different monomers. This complements recently reported degenerative transfer OMRP of vinyl acetate by a CoSal^{tBu,tBu} complex.[49] Of note, DT-OMRP is outside the scope of this initial report on electronic effects as we wished to examine the strength of the cobalt–carbon bond directly, not through associative exchange.

Table 5 Styrene polymerisation data for CoSal^{tBu,R2} [a]

CoSal^{tBu,R2}	% Conv.	$M_{n,th}$	M_n	PDI
$R_2 = NO_2$	55	5340	4630	2.23
$R_2 = tBu$	61	5880	5800	1.78
$R_2 = OMe$	72	6770	14 310	2.38
$R_2 = NMe_2$	85	7920	9110	1.65

[a] Bulk styrene polymerisations, 1 h at 120 °C, initiated with AIBN with complex : initiator : monomer ratio of 1 : 0.6 : 100. $M_{n,th} = [M]_0/2[I]_0 \times$ MW(monomer) × conversion + MW(catalyst).

Reversible termination OMRP of styrene. Variation of the *para* substituent in CoSal^{tBu,R2} complexes had an interesting effect on the behaviour of the complexes in the RT-OMRP of styrene (Table 5). As the substituents became more electron-donating, conversion increased (from 55% in 1 h for CoSal^{tBu,NO2} to 85% in 1 h for CoSal^{tBu,NMe2}). The increased electron density around the metal centre can explain this trend, as it would lower the favourability of the formation of the dormant species and increase propagating radical concentrations. Mulliken population analysis of the Co(II) derivatives shows increasing partial charge at Co, as expected based on the electron-donating ability of the *para*-ring substituents. Thus CoSal^{tBu,NO2} is predicted to have the most Lewis acidic metal centre of the series and also the highest Co(III)–carbon BDE. Molecular weights were in reasonable agreement with the theoretical values for the slower, less electron-rich complexes CoSal^{tBu,NO2} and CoSal^{tBu,tBu}, but much greater deviations between theoretical and experimental values were observed with the more electron-donating OMe and NMe_2 substituents in CoSal^{tBu,OMe} and CoSal^{tBu,NMe2} complexes. In all cases, the PDIs were broad (1.65–2.38), indicating that these polymerisations were not well-controlled and suggesting that irreversible termination reactions were prevalent. While reversible formation of cobalt–carbon bonds controlled the polymerisation under these conditions, classic metrics of controlled polymerisation were not observed, unlike the recently reported DT-OMRP of vinyl acetate.[49] We hypothesised that both the steric bulk of the *ortho* *t*Bu groups and the increased reaction temperature relative to the DT-OMRP conditions of 60 °C could play a role in limiting RT-OMRP control.

To investigate whether the steric bulk of the *t*Bu group at the *ortho* position of the aromatic ring was hindering the deactivation equilibrium and causing the broadened PDIs, we synthesised CoSal^{H,tBu} and screened it for styrene OMRP. 58% conversion in 1 h was obtained, with molecular weights which were slightly lower than theoretical values ($M_{n,th}$ = 5500, M_n = 4320) and an improved, but still broad, PDI of 1.65. This suggested that the bulk at the *ortho* position played, at most, a minor role in controlling the OMRP equilibrium.

To study whether the high polymerisation temperatures of 120 °C were favouring side reactions and thus broadening polydispersities, we investigated styrene polymerisation using V-70 as the initiator (Table S1, ESI‡). As expected, conversions

were lower at 65 °C, as the dormant species is favoured and propagation rates are reduced. PDIs were actually broader, with more deviation between theoretical and experimental molecular weights indicating that the lower temperatures were not preventing termination reactions. The productive, if uncontrolled, polymerisation at this lower temperature is also suggestive that the monomer scope of DT-OMRP by CoSal^{tBu,tBu} may be limited to monomers that form stronger cobalt–carbon bonds at these temperatures.

Despite reasonable agreement of experimental molecular weights with the theoretical values, the broad PDIs of 1.6–2.4 indicated that styrene polymerisation was inadequately controlled by Co complexes CoSal^{R1,R2}. To further investigate this, we examined kinetic data for the polymerisation of styrene by CoSal^{tBu,tBu}. Although the plot of $\ln([M]_0/[M]_t)$ was linear for the first 2 hours (Fig. 6a), with $k_{obs.} = 0.40\ h^{-1}$, deviations after this time indicated that the radical concentration did not remain constant. Interestingly, after just 10 minutes the conversion was 36%, indicating an initial rapid period of polymerisation where molecular weights quickly reached *ca.* 5500 Da. Molecular weights then increased in a linear fashion for the first hour, up to *ca.* 7200 Da at 56%. However, after this point the molecular weights stagnated, remaining at around 7000 Da for the rest of the polymerisation (Fig. 6b). This behaviour suggested the occurrence of catalytic chain transfer, which was confirmed by the presence of olefin end-groups at δ 6.2 ppm in the ^{1}H NMR spectra of the polymer samples (Fig. S4, ESI‡). Many cobalt(II) complexes are excellent CCT catalysts, particularly the cobaloximes and cobalt porphyrins,[69,70] and it is likely that a low metal–carbon bond dissociation energy in the polymerisation of styrene results in high radical concentrations which, coupled with a high concentration of Co(II), favours β-hydrogen abstraction. Reinitiation from the metal-hydride species gives new propagating chains, resulting in the broad PDIs which increase from 1.62 at early stages of the polymerisation to 2.04 at 80% conversion. Importantly, by altering the monomer concentration we can tune the 'top-out' molecular weight of our olefin-terminated polymer chains. For instance, with 500 eq. of monomer the molecular weights are increased to *ca.* 20 000 Da, achieved from 25% conversion onwards (Fig. S5, ESI‡). These moderate-length, olefin-terminated poly(styrene) chains could potentially be used as building blocks for extended macromolecular structures and offer an alternative to the short-chain oligomers traditionally synthesised through efficient CCT polymerisations. Attempted controlled radical polymerisations mediated by molybdenum[71,72] and iron[73–75] catalysts have previously been reported to yield olefin-terminated poly(styrene) through CCT processes, with the molecular weights of the polymers obtained typically *ca.* 1000–5000 Da.

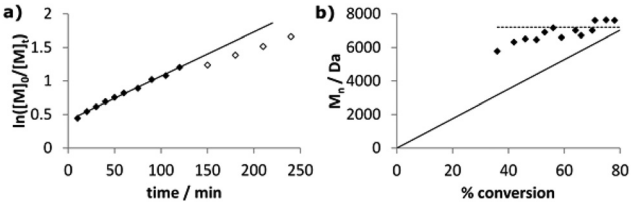

Fig. 6 Plots of (a) $\ln([M]_0/[M]_t)$ *vs.* time and (b) molecular weight *vs.* conversion for bulk styrene polymerisation at 120 °C using CoSal^{tBu,tBu} and AIBN. Monomer : catalyst : initiator ratio of 100 : 1 : 0.6 used. Solid data points in (a) used to calculate least-squares fit. Solid line in (b) represents $M_{n,th}$, while dashed line indicates 'top-out' molecular weight.

Monomer scope. The polymerisation of the more reactive methyl methacrylate monomer using CoSal^{tBu,tBu} proceeded rapidly (70% conversion in 15 minutes) and yielded molecular weights which were significantly lower than the theoretical values, with surprisingly narrow PDIs (*ca.* 1.24). Examination of crude samples revealed multimodal GPC traces, with the loss of much of the low molecular weight fraction during precipitation resulting in much narrower polydispersity traces in the worked-up samples (Fig. S6, ESI‡). Catalytic chain transfer was confirmed by the presence of olefin end-groups in the PMMA samples, at δ = 5.47 and 6.20 ppm. The well-established propensity for the methyl methacrylate monomer to undergo catalytic chain transfer reactions[69,70] is supported by the formation of this lower molecular weight polymer.

Building from the recently published work on the DT-OMRP of vinyl acetate by a cobalt salen complex (CoSal^{tBu,tBu}),[49] we also examined the four CoSal^{tBu,R2} complexes for the RT-OMRP of vinyl acetate (Table 6). Although a notoriously difficult monomer to control due to the difficulty in activating the monomer and then controlling the equilibrium between the unstabilised radical and the dormant species, vinyl acetate has been successfully polymerised using Co(acac)$_2$ and other Co-systems using both V-70 and AIBN initiators.[19,20,22] We anticipated that the formation of a stronger metal–carbon bond between the vinyl acetate radical and the Co complex would either hinder CCT and favour controlled radical polymerisation or, as expected for a system operating solely by DT-OMRP, form no polymeric products.

Complex CoSal^{tBu,NO2} was an unsuccessful mediator of VAc OMRP, with only small amounts of very high molecular weight polymer isolated. The strong electron-withdrawing substituent makes the Co centre electron-poor and irreversible binding of the vinyl acetate monomer to the complex is likely to occur, with a small amount of thermal polymerisation yielding the observed high molecular weight polymer. As observed with the styrene system, as more electron-donating substituents were incorporated into the CoSal^{tBu,R2} complexes, monomer conversion increased. However, the substituent effect on

Table 6 Vinyl acetate polymerisation data for complexes CoSal^{tBu,R2} [a]

Complex	% Conv.	$M_{n,th}$	M_n	PDI
$R_2 = NO_2$	17	1850	338 300	1.81
$R_2 = tBu$	49	4260	1280	1.61
$R_2 = OMe$	48	4130	4720	1.29
$R_2 = NMe_2$	50	4310	4240	1.60

[a] Bulk vinyl acetate polymerisations, 3 h at 120 °C, initiated with AIBN with complex : initiator : monomer ratio of 1 : 0.6 : 100. $M_{n,th} = [M]_0/2[I]_0 \times MW(monomer) \times conversion + MW(catalyst)$.

polymerisation rate was less profound for vinyl acetate, with complexes where R_2 = *t*Bu, OMe and NMe_2 all yielding *ca.* 50% conversion in 3 hours. More interesting was the effect on the molecular weight data, with complex $CoSal^{tBu,tBu}$ yielding molecular weights which were significantly lower than theoretical values. Complexes $CoSal^{tBu,OMe}$ and $CoSal^{tBu,NMe2}$ both gave poly(vinyl acetate) with molecular weights which were in good agreement with the theoretical values, although the PDI of 1.29 obtained with complex $CoSal^{tBu,OMe}$ suggests that the OMe substituent yields the optimal $CoSal^{tBu,R2}$ electronic structure out of this series. However, the reported molecular weight represented only 80% of the sample, with a higher molecular weight peak at *ca.* 97 000 Da making up the other 20%. We thought this was likely to be due to an inefficient deactivation process, allowing some chains to propagate in an uncontrolled manner, and so reduced the radical concentration. Using 0.5 equivalents of AIBN produced the same bimodal distribution (Table S2, ESI‡), with PDIs of 1.30 and 1.69 for the low and high molecular weight peaks, but reducing the amount of initiator further did yield a monomodal distribution. With 0.4 eq. of AIBN, conversion was 39% in 3 h (lower radical concentrations resulting in slower polymerisation) and the observed molecular weight of 4300 was in good agreement with the $M_{n,th}$ of 4765, with the PDI of 1.33 illustrating the reasonable control exerted over VAc OMRP by $CoSal^{tBu,OMe}$.

Removing the steric bulk of the *t*Bu group at the *ortho* position of the aromatic ring did not improve the control over VAc polymerisation. Complex $CoSal^{H,tBu}$ behaved similarly to complex $CoSal^{tBu,tBu}$, reaching 44% conversion in 3 h and yielding PVAc of lower molecular weight than the theoretical value (M_n = 1010, $M_{n,th}$ = 3780), but the increased PDI of 2.65 (*cf.* PDI of 1.61 for $CoSal^{tBu,tBu}$) indicated less control over the polymerisation.

Conclusions

A series of cobalt salen complexes have been prepared and studied by single crystal X-ray diffraction, cyclic voltammetry, X-ray photoelectron spectroscopy, electron paramagnetic resonance spectroscopy and computational methods. Characterisation supports a reactive metal centre tailored by altering ligand electronics. Electrochemistry showed an inverse correlation between redox potentials and electron-donating ability, corroborated by a decrease in the Co $2p_{3/2}$ and $2p_{1/2}$ binding energies measured by XPS. Tuning the framework was further evident in the theoretical calculations, in particular, the NO_2 derivative exhibited the highest Co(III)–carbon bond dissociation energy.

These initial results from RT-OMRP using $CoSal^{R1,R2}$ illustrate the potential of these complexes in controlled radical polymerisation. The data show that the cobalt–carbon bond strength varies with the ligand substitution and, while we could not achieve well-controlled styrene polymerisation under the conditions studied, our current work focuses on degenerative transfer OMRP. Monomers which are susceptible to β-hydrogen abstraction, including styrene, may be successfully polymerised at the lower temperatures used in DT-OMRP and we are particularly interested in studying the effects of our electron-donating and electron-withdrawing ligand substituents on the rate of VAc polymerisation with complexes $CoSal^{R1,R2}$ under DT-OMRP conditions. The RT-OMRP regime will be used for the synthesis of specific molecular weight, olefin-terminated polymer chains with a wide scope of monomers.

Experimental

Materials and methods

All chemicals used were of the highest grade available and were further purified whenever necessary.[76] Literature methods were followed to prepare Schiff-base ligands[50–54] $H_2Sal^{tBu,NO2}$, $H_2Sal^{tBu,tBu}$, $H_2Sal^{tBu,OMe}$, $H_2Sal^{tBu,NMe2}$, and $H_2Sal^{H,tBu}$ and Co complexes[50,53,55] $CoSal^{tBu,tBu}$, $CoSal^{tBu,OMe}$, and $CoSal^{H,tBu}$ Monomers styrene, methyl methacrylate, methyl acrylate and vinyl acetate were purchased from Aldrich Chemical Co. and dried by stirring over calcium hydride for 24 hours, before being vacuum transferred, degassed and stored at −35 °C under inert atmosphere. Azobis(isobutyronitrile), AIBN, was purchased from Aldrich, recrystallised from methanol prior to use and then stored at −35 °C under inert atmosphere. V-70 was purchased from Wako and used as received. ^{1}H NMR and 2-D spectra were recorded at 298 K with a Bruker Avance Spectrometer (300 MHz) in $CDCl_3$. Cyclic voltammetry (CV) was performed on a PAR-263A potentiometer, equipped with a Ag wire reference electrode, a platinum disk working electrode, and a Pt counter electrode with 0.1 M NBu_4ClO_4 solutions in CH_2Cl_2. Decamethylferrocene was used as an external standard, and redox processes assigned to the Co complexes were directly referenced to the standard. The redox potential for decamethylferrocene is reported as −0.59 V *vs.* ferrocene.[77] Mass spectra (positive ion) were obtained on an Agilent 6210 TOF ESI-MS instrument. All EPR spectra were collected using a Bruker EMXplus spectrometer operating with a premiumX X-band (~9.5 GHz) microwave bridge. Low temperature measurements of frozen solutions used a Bruker helium temperature-control system and a continuous flow cryostat. Samples for X-band measurements were placed in 4 mm outer-diameter sample tubes with sample volumes of ~300 μL. EPR spectra were simulated with EasySpin 4.0.0 software.[78] X-ray photoelectron spectra were obtained using a Kratos Analytical Axis ULTRA spectrometer containing a DLD detector. Gel permeation chromatography (GPC) was carried out in THF (flow rate: 1 mL min^{-1}) at 50 °C with a Polymer Labs PL-GPC 50 Plus integrated GPC system with two 300 × 7.8 mm Jordi gel DVB mixed bed columns, utilising a refractive index detector coupled with a Wyatt Technology miniDAWN™ TREOS® multiple angle light scattering (MALS) detector operating at 658 nm. Literature dn/dc values of 0.185, 0.088, 0.063 and 0.052 for poly(styrene),[79] poly(methyl methacrylate),[80] poly(methyl acrylate)[81] and poly(vinyl acetate),[79] respectively, were used.

Synthesis

Synthesis of CoSal^{tBu,NO2}. To a solution of $H_2Sal^{tBu,NO2}$ (110 mg, 0.21 mmol) dissolved in degassed Et_2O (5 mL) was added a solution of $Co(OAc)_2{\cdot}4H_2O$ (50 mg, 0.20 mmol) in degassed MeOH (5 mL). This mixture was stirred under N_2 for 15 minutes, in which time an orange precipitate formed. The solid was collected by filtration and was washed with MeOH, then dried under reduced pressure overnight. The resulting orange solid was recrystallised from THF–pentane (1 : 1) to afford long dark red crystals of CoSal^{tBu,NO2}·THF (63 mg, 46% yield). MS-ESI *m*/*z* (%): 582.2 (100) $[CoSal^{tBu,NO2}]^+$. Anal. calcd (found) for $C_{28}H_{34}N_4O_6Co{\cdot}THF$: C 58.80 (58.77), H 6.48 (6.61), N 8.57 (8.65).

Synthesis of CoSal^{tBu,NMe2}. To a solution of $H_2Sal^{tBu,NMe2}$ (95 mg, 0.18 mmol) dissolved in degassed MeOH (3 mL) was added a solution of $Co(OAc)_2{\cdot}4H_2O$ (45 mg, 0.22 mmol) in degassed MeOH (3 mL). This mixture was stirred under N_2 overnight, while a dark precipitate formed. The solid was collected by filtration and was dried under reduced pressure overnight to afford a dark green precipitate of CoSal^{tBu,NMe2} (43 mg, 41% yield). MS-ESI *m*/*z* (%): 577.3 (100) $[CoSal^{tBu,NMe2}]^+$. Anal. calcd (found) for $C_{32}H_{46}N_4O_2Co{\cdot}H_2O$: C 64.52 (64.39), H 8.12 (7.84), N 9.41 (9.41).

X-ray analysis

Single crystal X-ray crystallographic analysis of CoSal^{tBu,NO2} was performed on a Bruker X8 APEX II diffractometer with graphite monochromated Mo-Kα radiation. A dark red needle crystal of $C_{28}H_{34}N_4O_6Co{\cdot}THF$, isolated from the slow evaporation of a THF–pentane solution was mounted on a glass fibre. The data were collected at a temperature of −100.0 ± 0.1 °C to a maximum 2θ value of 55.0°. Data were collected in a series of ϕ and ω scans in 0.50° oscillations with 10.0-second exposures. The crystal-to-detector distance was 36.00 mm. The structure was solved by direct methods.[82] The material crystallises with 1 molecules of THF in the asymmetric unit. All non-hydrogen atoms were refined anisotropically. All C–H hydrogen atoms were placed in calculated positions but were not refined. All crystal structure plots were produced using ORTEP-3. A summary of the crystal data and experimental parameters for structure determinations are given in Table S4.‡

Calculations

Geometry optimisations were performed using the Gaussian 09 program (Revision A.02),[83] the B3LYP functional,[84,85] and the 6-31g* basis set on all atoms. Frequency calculations at the same level of theory confirmed that the optimised structures were located at a minimum on the potential energy surface. Single point calculations were performed using the same functional and the TZVP basis set of Ahlrichs[86,87] on all atoms. The corresponding orbital transformation (COT) was used to determine the singularly occupied molecular orbital for each of the Co complexes.[88,89] AOMix[90–92] was used for determining atomic orbital compositions employing Mulliken Population Analysis. Bond dissociation energies were calculated using the BP86 functional,[64] and the TZVP basis set following a published procedure.[65–67] The XYZ coordinates of the optimised structures are provided in the ESI.‡

Polymerisations

General polymerisation procedure for screening reactions. Monomer, catalyst and initiator in the ratio 100 : 1 : 0.6 were placed in an ampoule under inert atmosphere. The ampoule was stirred in a preheated oil-bath at the desired temperature for the required length of time, then removed from the heat and cooled quickly under running water. Work-up procedures were dependent on the monomer: poly(styrene), poly(methyl methacrylate) and poly(methacrylate) samples were dissolved in 5 mL of THF and precipitated into 150 mL of acidified methanol (1% HCl). Monomer conversion for these reactions was determined by ^{1}H NMR spectroscopic analysis of crude samples, by comparing the integration of the polymer *versus* monomer resonances. For poly(vinyl acetate), excess monomer was removed under reduced pressure, the samples were dried to constant mass and then weighed to determine monomer conversion gravimetrically.

Representative polymerisation procedure. CoSal^{tBu,tBu} (0.06 g, 0.1 mmol), AIBN (0.01 g, 0.06 mmol) and styrene (1.0 g, 10 mmol) were added to an ampoule containing a micro-stirrer bar under inert atmosphere, which was then sealed and heated at 120 °C with stirring for 1 h. ^{1}H NMR spectroscopic analysis of the crude residue indicated 61% monomer conversion, with GPC analysis of the crude material giving an M_n of 5800 and a PDI of 1.78. Precipitation into acidified methanol gave white poly(styrene), with M_n = 7020 and PDI = 1.58.

General polymerisation procedure for styrene kinetics. Monomer, catalyst and initiator in the desired ratio were placed in a Schlenk flask under inert atmosphere and sealed with a rubber septum (Suba-Seal^{tM}). The Schlenk flask was placed in an oil-bath preheated to 120 °C, at which point timing commenced. Samples were removed from the Schlenk *via* a degassed syringe at designated intervals and quenched with $CDCl_3$. Analysis of the crude samples by ^{1}H NMR spectroscopy gave the monomer conversion, while GPC analysis gave the molecular weights and PDIs of the samples.

Acknowledgements

This work is supported by an NSERC Discovery Grant and the University of Edinburgh (M. S.) and an NSERC Discovery Grant (T. S.). Compute Canada and Westgrid are thanked for access to computational resources.

Notes and references

1 R. Irie, K. Noda, Y. Ito, N. Matsumoto and T. Katsuki, *Tetrahedron Lett.*, 1990, **31**, 7345–7348.

2 E. N. Jacobsen, W. Zhang, A. R. Muci, J. R. Ecker and L. Deng, *J. Am. Chem. Soc.*, 1991, **113**, 7063–7064.
3 L. Canali and D. C. Sherrington, *Chem. Soc. Rev.*, 1999, **28**, 85–93.
4 P. G. Cozzi, *Chem. Soc. Rev.*, 2004, **33**, 410–421.
5 D. J. Darensbourg, R. M. Mackiewicz, A. L. Phelps and D. R. Billodeaux, *Acc. Chem. Res.*, 2004, **37**, 836–844.
6 E. M. McGarrigle and D. G. Gilheany, *Chem. Rev.*, 2005, **105**, 1563–1602.
7 D. J. Darensbourg, *Chem. Rev.*, 2007, **107**, 2388–2410.
8 D. J. Darensbourg, in *Synthetic Biodegradable Polymers*, ed. B. Rieger, A. Kunkel, G. W. Coates, R. Reichardt, E. Dinjus and T. A. Zevaco, 2012, vol. 245, pp. 1–27.
9 X.-B. Lu and D. J. Darensbourg, *Chem. Soc. Rev.*, 2012, **41**, 1462–1484.
10 E. N. Jacobsen, *Acc. Chem. Res.*, 2000, **33**, 421–431.
11 W. Hirahata, R. M. Thomas, E. B. Lobkovsky and G. W. Coates, *J. Am. Chem. Soc.*, 2008, **130**, 17658–17659.
12 R. M. Thomas, P. C. B. Widger, S. M. Ahmed, R. C. Jeske, W. Hirahata, E. B. Lobkovsky and G. W. Coates, *J. Am. Chem. Soc.*, 2010, **132**, 16520–16525.
13 G. W. Coates and D. R. Moore, *Angew. Chem., Int. Ed.*, 2004, **43**, 6618–6639.
14 E. N. Jacobsen, W. Zhang and M. L. Guler, *J. Am. Chem. Soc.*, 1991, **113**, 6703–6704.
15 M. Palucki, N. S. Finney, P. J. Pospisil, M. L. Guler, T. Ishida and E. N. Jacobsen, *J. Am. Chem. Soc.*, 1998, **120**, 948–954.
16 H. Jacobsen and L. Cavallo, *Chem.–Eur. J.*, 2001, **7**, 800–807.
17 Z. Qin, C. M. Thomas, S. Lee and G. W. Coates, *Angew. Chem., Int. Ed.*, 2003, **42**, 5484–5487.
18 D. J. Darensbourg, R. M. Mackiewicz, J. L. Rodgers, C. C. Fang, D. R. Billodeaux and J. H. Reibenspies, *Inorg. Chem.*, 2004, **43**, 6024–6034.
19 L. E. N. Allan, M. R. Perry and M. P. Shaver, *Prog. Polym. Sci.*, 2012, **37**, 127–156.
20 A. Debuigne, R. Poli, C. Jérôme, R. Jérôme and C. Detrembleur, *Prog. Polym. Sci.*, 2009, **34**, 211–239.
21 F. di Lena and K. Matyjaszewski, *Prog. Polym. Sci.*, 2010, **35**, 959–1021.
22 M. Hurtgen, C. Detrembleur, C. Jérôme and A. Debuigne, *Polym. Rev.*, 2011, **51**, 188–213.
23 M. P. Shaver, M. E. Hanhan and M. R. Jones, *Chem. Commun.*, 2010, **46**, 2127–2129.
24 M. R. Perry, L. E. N. Allan, A. Decken and M. P. Shaver, *Dalton Trans.*, 2013, **42**, 9157–9165.
25 Z. Xue and R. Poli, *J. Polym. Sci., Part A: Polym. Chem.*, 2013, **51**, 3494–3504.
26 B. B. Wayland, G. Poszmik, S. L. Mukerjee and M. Fryd, *J. Am. Chem. Soc.*, 1994, **116**, 7943–7944.
27 B. B. Wayland, L. Basickes, S. Mukerjee, M. Wei and M. Fryd, *Macromolecules*, 1997, **30**, 8109–8112.
28 Z. Lu, M. Fryd and B. B. Wayland, *Macromolecules*, 2004, **37**, 2686–2687.
29 B. B. Wayland, C.-H. Peng, X. Fu, Z. Lu and M. Fryd, *Macromolecules*, 2006, **39**, 8219–8222.
30 B. Langlotz, J. Lloret Fillol, J. Gross, H. Wadepohl and L. Gade, *Chem.–Eur. J.*, 2008, **14**, 10267–10279.
31 A. Debuigne, J. R. Caille, C. Detrembleur and R. Jérôme, *Angew. Chem., Int. Ed.*, 2005, **44**, 3439–3442.
32 A. Debuigne, J. R. Caille and R. Jérôme, *Angew. Chem., Int. Ed.*, 2005, **44**, 1101–1104.
33 C. Detrembleur, A. Debuigne, R. Bryaskova, B. Charleux and R. Jérôme, *Macromol. Rapid Commun.*, 2006, **27**, 37–41.
34 V. Sciannamea, A. Debuigne, Y. Piette, R. Jérôme and C. Detrembleur, *Chem. Commun.*, 2006, 4180–4182.
35 S. Maria, H. Kaneyoshi, K. Matyjaszewski and R. Poli, *Chem.–Eur. J.*, 2007, **13**, 2480–2492.
36 A. Debuigne, Y. Champouret, R. Jérôme, R. Poli and C. Detrembleur, *Chem.–Eur. J.*, 2008, **14**, 4046–4059.
37 H. Kaneyoshi and K. Matyjaszewski, *Macromolecules*, 2005, **38**, 8163–8169.
38 M. Hurtgen, A. Debuigne, C. Jérôme and C. Detrembleur, *Macromolecules*, 2010, **43**, 886–894.
39 C. Detrembleur, D.-L. Versace, Y. Piette, M. Hurtgen, C. Jerome, J. Lalevee and A. Debuigne, *Polym. Chem.*, 2012, **3**, 1856–1866.
40 A. Debuigne, C. Michaux, C. Jérôme, R. Jérôme, R. Poli and C. Detrembleur, *Chem.–Eur. J.*, 2008, **14**, 7623–7637.
41 A. Debuigne, J. Warnant, R. Jérôme, I. Voets, A. de Keizer, M. A. Cohen Stuart and C. Detrembleur, *Macromolecules*, 2008, **41**, 2353–2360.
42 M. R. Buchmeiser and M. G. Marino, *Macromol. Mater. Eng.*, 2012, **297**, 894–901.
43 C. Detrembleur, A. Debuigne, O. Altintas, M. Conradi, E. H. H. Wong, C. Jerome, C. Barner-Kowollik and T. Junkers, *Polym. Chem.*, 2012, **3**, 135–147.
44 H. Kaneyoshi and K. Matyjaszewski, *Macromolecules*, 2006, **39**, 2757–2763.
45 D. N. Bunck, G. P. Sorenson and M. K. Mahanthappa, *J. Polym. Sci., Part A: Polym. Chem.*, 2011, **49**, 242–249.
46 A. Debuigne, N. Willet, R. Jérôme and C. Detrembleur, *Macromolecules*, 2007, **40**, 7111–7118.
47 K. S. S. Kumar, Y. Li, Y. Gnanou, U. Baisch, Y. Champouret, R. Poli, K. C. D. Robson and W. S. McNeil, *Chem.–Asian J.*, 2009, **4**, 1257–1265.
48 R. K. Sherwood, C. L. Kent, B. O. Patrick and W. S. McNeil, *Chem. Commun.*, 2010, **46**, 2456–2458.
49 C.-M. Liao, C.-C. Hsu, F.-S. Wang, B. B. Wayland and C.-H. Peng, *Polym. Chem.*, 2013, **4**, 3098–3104.
50 W. H. Leung, E. Y. Y. Chan, E. K. F. Chow, I. D. Williams and S. M. Peng, *Dalton Trans.*, 1996, 1229–1236.
51 I. Sylvestre, J. Wolowska, C. A. Kilner, E. J. L. McInnes and M. A. Halcrow, *Dalton Trans.*, 2005, 3241–3249.
52 Y. N. Belokon, W. Clegg, R. W. Harrington, M. North and C. Young, *Inorg. Chem.*, 2008, **47**, 3801–3814.
53 A. Kochem, H. Kanso, B. Baptiste, H. Arora, C. Philouze, O. Jarjayes, H. Vezin, D. Luneau, M. Orio and F. Thomas, *Inorg. Chem.*, 2012, **51**, 10557–10571.
54 L. Chiang, A. Kochem, O. Jarjayes, T. J. Dunn, H. Vezin, M. Sakaguchi, T. Ogura, M. Orio, Y. Shimazaki, F. Thomas and T. Storr, *Chem.–Eur. J.*, 2012, **18**, 14117–14127.

55 R. I. Kureshy, K. J. Prathap, S. Agrawal, M. Kumar, N. U. H. Khan, S. H. R. Abdi and H. C. Bajaj, *Eur. J. Org. Chem.*, 2009, 2863–2871.
56 T. Kurahashi and H. Fujii, *Inorg. Chem.*, 2013, **52**, 3908–3919.
57 C. A. Bessel and D. R. Rolison, *J. Phys. Chem. B*, 1997, **101**, 1148–1157.
58 V. D. Chaube, S. Shylesh and A. P. Singh, *J. Mol. Catal. A: Chem.*, 2005, **241**, 79–87.
59 Y.-S. Kim, C.-Y. Lee and G.-J. Kim, *Bull. Korean Chem. Soc.*, 2010, **31**, 2973–2979.
60 C. Daul, C. W. Schläpfer and A. von Zelewsky, *Struct. Bonding*, 1979, **36**, 129–171.
61 E. Vinck, S. Van Doorslaer, D. M. Murphy and I. A. Fallis, *Chem. Phys. Lett.*, 2008, **464**, 31–37.
62 R. S. Mulliken, *J. Chem. Phys.*, 1955, **23**, 1833–1840.
63 I. G. Csizmadia, *Int. J. Quantum Chem.*, 1978, **13**, 159–159.
64 J. P. Perdew, *Phys. Rev. B: Condens. Matter*, 1986, **33**, 8822–8824.
65 J. Kuta, S. Patchkovskii, M. Z. Zgierski and P. M. Kozlowski, *J. Comput. Chem.*, 2006, **27**, 1429–1437.
66 P. M. Kozlowski, J. Kuta and W. Galezowski, *J. Phys. Chem. B*, 2007, **111**, 7638–7645.
67 W. Galezowski, J. Kuta and P. M. Kozlowski, *J. Phys. Chem. B*, 2008, **112**, 3177–3183.
68 G. Li, F. F. Zhang, H. Chen, H. F. Yin, H. L. Chen and S. Y. Zhang, *Dalton Trans.*, 2002, 105–110.
69 A. A. Gridnev and S. D. Ittel, *Chem. Rev.*, 2001, **101**, 3611–3660.
70 J. P. A. Heuts and N. M. B. Smeets, *Polym. Chem.*, 2011, **2**, 2407–2423.
71 E. Le Grognec, J. Claverie and R. Poli, *J. Am. Chem. Soc.*, 2001, **123**, 9513–9524.
72 S. Maria, F. Stoffelbach, J. Mata, J.-C. Daran, P. Richard and R. Poli, *J. Am. Chem. Soc.*, 2005, **127**, 5946–5956.
73 M. P. Shaver, L. E. N. Allan, H. S. Rzepa and V. C. Gibson, *Angew. Chem., Int. Ed.*, 2006, **45**, 1241–1244.
74 L. E. N. Allan, M. P. Shaver, A. J. P. White and V. C. Gibson, *Inorg. Chem.*, 2007, **46**, 8963–8970.
75 R. K. O'Reilly, M. P. Shaver, V. C. Gibson and A. J. P. White, *Macromolecules*, 2007, **40**, 7441–7452.
76 D. D. Perrin and W. L. F. Armarego, *Purification of Laboratory Chemicals*, Pergamon Press, New York, 1st edn, 1988.
77 N. G. Connelly and W. E. Geiger, *Chem. Rev.*, 1996, **96**, 877–910.
78 S. Stoll and A. Schweiger, *J. Magn. Reson.*, 2006, **178**, 42–55.
79 S. Grcev, P. Schoenmakers and P. Iedema, *Polymer*, 2004, **45**, 39–48.
80 K. Min, H. Gao, J. A. Yoon, W. Wu, T. Kowalewski and K. Matyjaszewski, *Macromolecules*, 2009, **42**, 1597–1603.
81 B. Metin and F. D. Blum, *J. Chem. Phys.*, 2006, **124**, 054908–054910.
82 A. Altomare, M. C. Burla, M. Camalli, G. L. Cascarano, C. Giacovazzo, A. Guagliardi, A. G. G. Moliterni, G. Polidori and R. Spagna, *J. Appl. Crystallogr.*, 1999, **32**, 115–119.
83 M. J. Frisch, G. W. Trucks, H. B. Schlegel, G. E. Scuseria, M. A. Robb, J. R. Cheeseman, G. Scalmani, V. Barone, B. Mennucci, G. A. Petersson, H. Nakatsuji, M. Caricato, X. Li, H. P. Hratchian, A. F. Izmaylov, J. Bloino, G. Zheng, J. L. Sonnenberg, M. Hada, M. Ehara, K. Toyota, R. Fukuda, J. Hasegawa, M. Ishida, T. Nakajima, Y. Honda, O. Kitao, H. Nakai, T. Vreven, J. J. A. Montgomery, J. E. Peralta, F. Ogliaro, M. Bearpark, J. J. Heyd, E. Brothers, K. N. Kudin, V. N. Staroverov, R. Kobayashi, J. Normand, K. Raghavachari, A. Rendell, J. C. Burant, S. S. Iyengar, J. Tomasi, M. Cossi, N. Rega, N. J. Millam, M. Klene, J. E. Knox, J. B. Cross, V. Bakken, C. Adamo, J. Jaramillo, R. Gomperts, R. E. Stratmann, O. Yazyev, A. J. Austin, R. Cammi, C. Pomelli, J. W. Ochterski, R. L. Martin, K. Morokuma, V. G. Zakrzewski, G. A. Voth, P. Salvador, J. J. Dannenberg, S. Dapprich, A. D. Daniels, Ö. Farkas, J. B. Foresman, J. V. Ortiz, J. Cioslowski and D. J. Fox, *Gaussian 09, Revision A.02*, Gaussian, Inc., Wallingford, CT, 2009.
84 A. D. Becke, *J. Chem. Phys.*, 1993, **98**, 5648–5652.
85 P. J. Stephens, F. J. Devlin, C. F. Chabalowski and M. J. Frisch, *J. Phys. Chem.*, 1994, **98**, 11623–11627.
86 A. Schafer, H. Horn and R. Ahlrichs, *J. Chem. Phys.*, 1992, **97**, 2571–2577.
87 A. Schafer, C. Huber and R. Ahlrichs, *J. Chem. Phys.*, 1994, **100**, 5829–5835.
88 D. Herebian, K. E. Wieghardt and F. Neese, *J. Am. Chem. Soc.*, 2003, **125**, 10997–11005.
89 F. Neese, *J. Phys. Chem. Solids*, 2004, **65**, 781–785.
90 S. I. Gorelsky and A. B. P. Lever, *J. Organomet. Chem.*, 2001, **635**, 187–196.
91 S. I. Gorelsky, *AOMix: Program for Molecular Orbital Analysis*, University of Ottawa, Canada, 2007, http://www.sg-chem.net/
92 S. I. Gorelsky and E. I. Solomon, *Theor. Chem. Acc.*, 2008, **119**, 57–65.